COMMUNICATION

Cyclic Triimidazole Derivatives: Intriguing Cases of Multiple Emissions and RT Ultralong Phosphorescence

Elena Lucenti,[a] Alessandra Forni,*[a] Chiara Botta,*[b] Lucia Carlucci,[c] Clelia Giannini,[c] Daniele Marinotto,[c] Alessandro Pavanello,[c] Andrea Previtali,[c] Stefania Righetto[c] and Elena Cariati*[c]

Abstract: Solid luminogens' performances are determined by both their inherent electronic properties and packing status. Intermolecular interactions have been exploited to produce persistent room-temperature phosphorescence (RTP) from organic molecules. However, the design of organic materials with bright RTP and the rationalization of the role of interchromophoric electronic coupling remain a challenging task. Cyclic triimidazole has been demonstrated as a promising scaffold due to its crystalline induced room temperature ultralong phosphorescence (RTUP) associated with H aggregation. Herein, we report three triimidazole derivatives representing a significant example of multifaceted emission. In particular, dual fluorescence, RTUP, phosphorescences from molecular and supramolecular units are observed. H aggregation is responsible for the red RTUP, Br atoms favour yellow molecular phosphorescence, while halogen bonded Br···Br tetrameric units are involved in the blue-green phosphorescence.

Organic emissive materials offer different advantages with respect to their organometallic counterparts mainly because they are environmentally safer and biologically more compatible, allowing a wide range of optical, electronic, and biological applications.[1] In spite of such good promises, the isolation of new organic luminogens characterized by multicolored emission with lifetimes spanning from ns to ms remains a quite challenging task. When dealing with new emitting materials, it is important to fully characterize not only the inherent luminogen's behavior but also the influence of the molecular environment since solid state luminogens may exhibit unexpected properties, much different from their behaviors in solutions, indicating the vital role of molecular packing and intermolecular interactions. Examples of luminogens' performances determined by both their inherent electronic properties and packing status are the current two hot topics of aggregation-induced emission (AIE)[2] and room-temperature phosphorescence (RTP).[3-7] One striking example where the combined use of heavy halogen atom effect and intermolecular electronic coupling[8] led to increased red organic RTP efficiency has been recently reported.[9]

We have recently reported a simple pure organic material, triimidazo[1,2-a:1',2'-c:1'',2''-e][1,3,5]triazine (TT), able to display crystallization induced and mechanochromic emissive behavior, together with room temperature ultralong phosphorescence (RTUP) at ambient conditions (1s)[10] associated with H-aggregation which provides the necessary stabilization of the triplet excitons.[11]

Based on these exciting results we have here extended our investigation to: benzo[4,5]imidazo[1,2-*a*]benzo[4,5]imidazo[1,2-*c*]benzo[4,5]imidazo[1,2-*e*][1,3,5]triazine (**1**), 3-bromotriimidazo[1,2-*a*:1',2'-*c*:1'',2''-*e*][1,3,5]triazine (**2**) and 3,7-dibromotriimidazo[1,2-*a*:1',2'-*c*:1'',2''-*e*][1,3,5]triazine (**3**). The three compounds are characterized by multiple emissions going from molecular fluorescence and phosphorescence (MP) to H aggregate RTUP. The nature of the emissions is verified and interpreted through complete steady-state and time resolved photophysical characterization in solution and crystalline powders in air (see Table 1), by structural determination and theoretical calculations. **1** was synthesized as reported in the literature[12] while the new compounds **2** and **3** were prepared by bromination of TT with *N*-bromosuccinimide (see SI for experimental details).

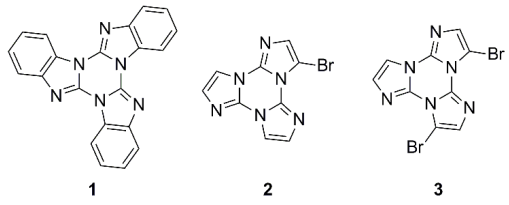

Scheme 1. Structure of cyclic triimidazoles **1**, **2** and **3**.

Diluted solutions of **1** ($2x10^{-5}$-$5x10^{-6}$M) in DCM display at RT a structured absorption spectrum with a maximum at 261 nm (ε=41213$M^{-1}cm^{-1}$) and a structured fluorescent emission (3.24ns, Figure S1, Φ=17%) at 327 and 340nm (Figure 1b and Table 1). At 77K only a minor red-shift in the emission is observed (Figure S2). Powders of **1** show at RT both dual fluorescence and phosphorescence (with 18% overall Φ). In fact, by exciting at 260nm, a near UV fluorescent emission resembling that of the chromophore in diluted solution is observed (Figure 1c Top), while by exciting at 370nm a red shifted manifold emission, resulting in white light, is detected (Figure 1a,c Bottom). In particular, a structured blue fluorescence centered at 407nm is superimposed to a RTUP (τ up to 0.5s, Figure S5) peaked at *ca.*

[a] Dr. E. Lucenti, Dr. A. Forni
ISTM-CNR, INSTM RU
via Golgi 19, 20133 Milano, Italy.
E-mail: alessandra.forni@istm.cnr.it
[b] Dr. C. Botta
ISMAC-CNR, INSTM RU
Via Corti 12, 20133 Milano, Italy.
E-mail: chiara.botta@ismac.cnr.it
[c] Prof. L. Carlucci, Dr. C. Giannini, Dr. D. Marinotto, Dr. A. Pavanello, Dr. A. Previtali, Dr. S. Righetto, Prof. E. Cariati
Dept. of Chemistry, Università degli Studi di Milano and INSTM RU
via Golgi 19, 20133 Milano, Italy.
E-mail: elena.cariati@unimi.it

Supporting information for this article is given via a link at the end of the document.

bout 530nm in the delayed spectrum (10 ms delay). At 77K a similar behavior is produced even though the blue fluorescence and the UP (which lasts for *ca.* 1s) become visible also by exciting at 260nm (Figure S6).

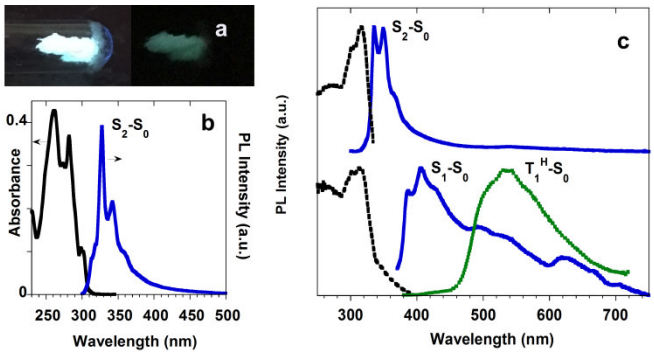

Figure 1. Compound **1**: **a)** Powders at 77K with UV on (left) and off (right); **b)** in DCM at RT: absorption and emission (blue line, λ_{exc}=380nm); **c)** powders at RT: Top: excitation (dashed black line, λ_{em}=348nm) and emission (blue line, λ_{exc}=260nm). Bottom: excitation (dashed black line, λ_{em}=408nm), emission (blue line, λ_{exc}=370nm) and phosphorescence (green dotted line, 10ms delay, window 510ms, λ_{exc}=358nm).

The TDDFT absorption spectrum of the optimized monomer **1** (see SI) shows a $S_0 \rightarrow S_1$ transition of $\pi \rightarrow \pi^*$ character at 255nm with zero oscillator strength, *f* (Table S2 and Figure S37) due to the high symmetry of the π–electron system. Two almost degenerate transitions are obtained at 238nm ($S_0 \rightarrow S_2$ and $S_0 \rightarrow S_3$, *f*=0.403), followed by other stronger transitions in good agreement with the measured UV spectrum. As previously reported for several other large conjugated molecules,[13] such electronic conditions are at the basis of $S_2 \rightarrow S_0$ emission (observed at 327nm). In the solid state the molecular symmetry is partially lost owing to intermolecular forces as previously demonstrated for TT,[10] allowing intensification of the $S_0 \rightarrow S_1$ transition. These results may explain the presence of dual fluorescence in the solid state: a stronger $S_2 \rightarrow S_0$ emission (at 335nm) and a weaker $S_1 \rightarrow S_0$ one (at 407nm) selectively activated by populating the S_1 state. Unfortunately, all attempts to prepare single crystals of **1** suitable for X-ray diffraction analysis failed, as also previously reported,[12] so that the origin of the RTP can only be guessed on the basis of the similarity of the photophysical behavior of **1** with that of parent TT.[10] For this latter compound the solid state RTUP was attributed to the presence of H aggregates whose formation is expected also in **1** originating a stabilized T_1^H level.

Diluted solutions of **2** ($5x10^{-5}$-$5x10^{-6}$M) in DCM (Figure 2b Top) display a very sharp and intense (ε=69360$M^{-1}cm^{-1}$) absorption band at 230nm with a shoulder at *ca.* 237nm and a low energy tail at *ca.* 250-280nm (see Table 1). A structured emission is observed at 328 and 342nm (τ_{av}=0.38ns, Figure S9; Φ=3%). At 77K by exciting over 300nm a very weak emission is observed at *ca.* 460nm (Figure S10). However, a very intense and broad MP centred at 580nm (τ_{av}=256μs, Figure S11) dominates the spectrum by exciting below 280nm (Figure 2b Bottom). The lifetime of this phosphorescence is unaffected by the presence/absence of O_2. Powders of **2**, when excited at 300nm at RT, are characterized by a structured emission at 326, 345 and 365nm (τ<1ns, Φ below instrumental sensitivity) very similar to that observed in solution (Figure 2c Top). Moreover, a second fluorescence centred at *ca.* 426nm is excited at 360nm (Figure 2c Bottom; τ_{av}=4ns, Figure S13). This behavior closely resembles that of **1** even though no RTUP is detected. By lowering the temperature, similar features are observed for excitation above 300nm, while by exciting at 280nm the spectrum is dominated by the MP at 575nm (Figure 2d; τ=274μs Figure S15).

Figure 2. Compound **2**: **a)** Crystal packing: π-π stacking interactions and Br···N XB in yellow and green dotted lines respectively; **b)** in DCM: Top: absorption and emission (λ_{exc}=280nm) at RT; Bottom: excitation (black dotted line, λ_{em}=580nm) and emission (red line, λ_{exc}=280nm) at 77K; **c)** powders at RT: Top: excitation (black dotted line, λ_{em}=363nm) and emission (blue line, λ_{exc}=300nm); Bottom: excitation (green dashed line, λ_{em}=429nm) and emission (red line, λ_{exc}=360nm); **d)** powders at 77K: Top: emission (green line, λ_{exc}=300nm) and excitation (blue line, λ_{em}=363nm; black dashed line, λ_{em}=492nm). Bottom: excitation (black dashed line, λ_{em}=580nm) and emission (red line, λ_{exc}=280nm red line).

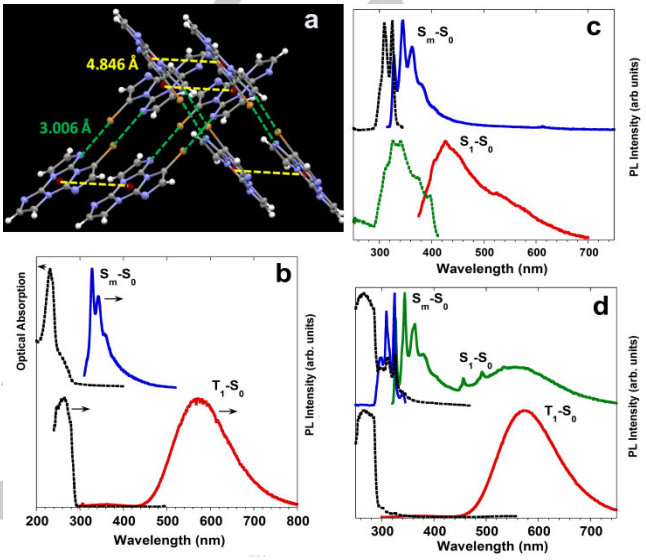

TDDFT calculations on monomeric **2** provide a weakly allowed $S_0 \rightarrow S_1$ transition of $\pi \rightarrow \pi^*$ character (*f*=0.024, at 231nm, Table S3) due to the presence of the bromine which disrupts the high symmetry of the π–electron system. Strong transitions are computed at 214, 208 and 204nm ($S_0 \rightarrow S_3$, f=0.203; $S_0 \rightarrow S_4$, f=0.400 and $S_0 \rightarrow S_5$, f=0.524, respectively), in perfect agreement with the experimental spectrum. The $S_0 \rightarrow S_2$ transition, computed at 219nm, is a symmetry forbidden $\pi \rightarrow \sigma^*$ excitation where the σ^* orbital is mainly delocalized on bromine and the C–Br bond. As in the case of **1**, calculations support multiple fluorescent emissions, with a stronger $S_m \rightarrow S_0$ (at 326nm, the only one visible in solution) and a weaker $S_1 \rightarrow S_0$ one (at 426nm) selectively activated by populating the S_1 state. Phosphorescence emission at 77K in both solution and solid state at *ca.* 580 nm activated by exciting below 280nm, is attributed to the presence of a T_n level (at 207nm, T_9 in Table S3) with $\sigma \rightarrow \sigma^*$ symmetry where the σ orbital is mainly localized on the bromine atom, which guarantees an efficient ISC (by both El Sayed and heavy atom effects) from the closest S_n levels (at 208 and 203nm, S_4 and S_5 in Table S3 respectively). IC to T_1 then leads to phosphorescent emission. Such interpretation

fully explains the experimental observation that phosphorescence is only produced by exciting below 280nm, the energy required to populate the proper S_n levels. Moreover, it supports the molecular origin of the phosphorescence. The absence of the UP in solid **2** agrees with the lacking of H aggregates in its structure as evidenced by single crystal XRD (Figure 2a and SI). In fact, **2** crystallizes in a π-stacked arrangement of largely shifted dimeric units (the distance between centroids of the triazinic rings is 4.846Å), self-assembled through a cyclic Br···N halogen-bonded (XB) motif. Adjacent stacks interact through weak C–H···N and C–H···π hydrogen bonds (HBs) along the molecular plane and in the direction perpendicular to it, respectively.

Figure 3. Compound **3**: **a)** Top: powders at 77K with under 360nm (left) and 254nm lamp (right); Bottom: Crystal packing: π-π stacking interactions and

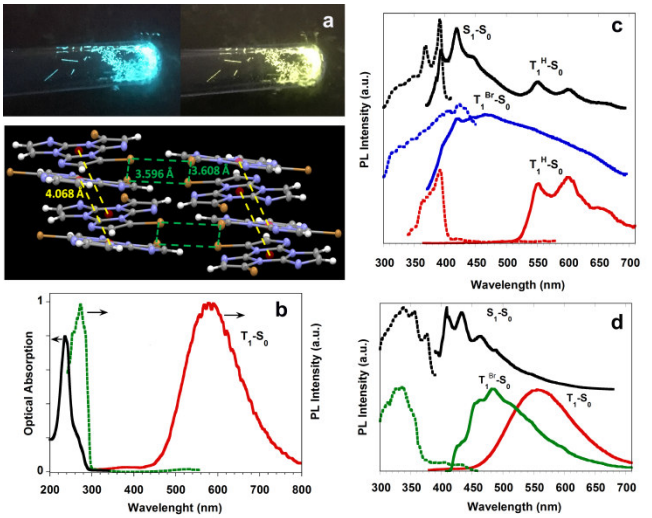

Br···Br XB in yellow and green dotted lines respectively; **b)** in DCM: absorption at RT (black line); excitation (green dashed line, λ_{em}=580nm) and emission (red line, λ_{exc}=280nm) at 77K; **c)** powders at RT: Top: excitation (black dotted line, λ_{em}=418nm) and emission (black line, λ_{exc}=355nm). Middle: excitation and phosphorescence emission (blue dashed line, λ_{em}=475nm; blue line, λ_{exc}=355nm, 5μs delay, window 0.1ms) Bottom: excitation and phosphorescence emission (red dashed line, λ_{em}=600nm; red line, λ_{exc}=355nm, 0.5ms delay, window 30ms); **d)** powders at 77K: Top: excitation (black dotted line, λ_{em}=410nm) and emission (black line, λ_{exc}=375nm). Bottom: excitation (green dashed line, λ_{em}=475nm), phosphorescence emission (green line, λ_{exc}=355nm, 0.5ms delay, window 30ms) and delayed emission (red line, λ_{exc}=265nm, 5μs delay, window 100μs)

Diluted solutions of **3** ($2.5x10^{-5}$-$5x10^{-6}$M) in DCM display a very sharp and intense (ε=36892$M^{-1}cm^{-1}$) absorption band at 235nm and a low energy tail at 250-280nm (Figure 3b and Table 1), with a hardly discernible emission at *ca.* 380nm (τ_{av}=3.48ns, Figure S17 and S18). At 77K, the emission spectrum is again dominated by the intense broad MP at 580nm (τ_{av}=265μs unaffected by the presence/absence of oxygen, Figure S19) which is excited only at wavelengths below 280nm (Figure 3b). Powders of **3** are characterized by a rather complicated emissive behavior. At RT a structured fluorescence at 395, 419 and 443nm (Figure 3c, τ_{av}=0.71ns, Figure S20), a broad long-lived component (*ca.* 470nm, τ up to 1.25ms, Figure S21) only distinguishable in the delayed spectrum and a structured RTUP (553, 600nm, τ up to 49ms, Figure S22) with 14% overall Φ, are detected. However, it is important to mention that the relative intensity of the RTUP increases with increasing crystallinity of the sample. At 77K (Figure 3d), a structured fluorescence at 409, 434 and 462nm (τ_{av}=1.51ns, Figure S23) very similar to the RT one appears when exciting at 375nm (Figure 3d Top); a long phosphorescence at 461, 484nm (τ_{av}=3.59ms, Figure S24) is observed by exciting at 355nm and the MP at 558nm (τ=302μs, Figure S25) dominates the spectrum by exciting below 280nm (Figure 3d Bottom). Importantly, the long phosphorescence at *ca.* 480nm, differently from the RTUP at 553nm, is rather insensitive to the degree of crystallinity of the sample. To better analyze this aspect, the behavior of relatively high loading thin films of the luminogens in PMMA (10%w/w) has been studied (Figure S26 and S27). For **3**/PMMA films, the RTUP is lacking as expected while the 480nm long-lived one is visible only working in the absence of oxygen (Figure S28). By exciting below 280nm, the 580nm MP is turned on only decreasing the temperature. It appears at 200K and at 180K it overcomes the 480nm long-lived component becoming the only visible at 77K (Figure S27). This behavior clearly indicates a completely different origin for the three phosphorescences.

TDDFT calculations provide two weakly allowed ($S_0 \rightarrow S_1$, *f*=0.016, at 233nm, and $S_0 \rightarrow S_4$, f=0.067, at 215nm, Table S4) and two symmetry-forbidden ($S_0 \rightarrow S_2$ and $S_0 \rightarrow S_3$) transitions in between, all of $\pi \rightarrow \pi^*$ character, supporting the very weak emission from the molecule at RT. The presence at 77K both in solution and in the solid state of the MP at *ca.* 570nm activated by exciting below 280nm, is, as in the case of **2**, explained by the presence of a T_n level (at 207nm, T_{10} in Table S4) with $\sigma \rightarrow \sigma^*$ symmetry and Br character. However, differently from **2**, powders of **3** display RTUP ($T_1^H \rightarrow S_0$) associated with the presence of H aggregates in the structure as confirmed by XRD (Figure 3a and SI). Crystal structure of **3** consists of slightly corrugated planes where molecules are arranged in tetrameric Br···Br XB cyclic units (Br_4-synthon)[14] which stack along the a-axis with a quite limited lateral shift (the distance between centroids of the triazinic rings is 4.068Å), similar to what observed for TT. The Br_4-synthon shows a 'Type II' geometrical disposition due to the electrostatic nature of XB:[15] the positive σ-hole located on each halogen X along the extension of the C–X bond points towards the negative belt around the adjacent X atom. Within the planes, tetrameric units are connected through C–H···N HBs and Br···N XB. Differently from **1** and TT, the presence of the XB motif in the molecular plane is probably responsible, as reported for other Br···Br aggregates,[16] of an additional deactivation channel ($T_1^{Br} \rightarrow S_0$) which is sensitive to thermal vibrations and oxygen at RT but becomes predominant at 77K. Structural studies indicate cell volume contraction of 2.6% at 120K (see SI) associated with a Br···Br shortening of 0.0501(5) and 0.0777(5)Å and a distance between triazinic centroids reduced by 0.078(2)Å.

In conclusion, the effectiveness of the simple TT scaffold[10] to produce manifold emissive behavior is here highlighted. The multiple emissions of the three triimidazole derivatives have been elucidated according to the diagram reported in Figure 4. Analogously to other organic luminogens, dual fluorescence with a component originated from S_2 and S_m is observed for **1** and **2**, respectively, due to the larger oscillator strength of higher energy singlet levels. The unprecedented behavior of brominated **2** and **3** with bright yellow MP activated at high energy (below 280nm)

excitation at 77K is associated with the presence of a T_n level of proper symmetry and close to a high energy S_n level. Selectively populating this S_n level, molecular emission from T_1 is observed. Solid state RTUP observed for **1** and **3** is attributed to the presence of a stabilized T_1^H level, while the additional phosphorescence of **3,** quenched by oxygen and quite sensitive to thermal vibrations, is associated with a T_1^{Br} level. The origin of the blue, blue-green, yellow and red emissions of this class of molecules is associated with different excited states with markedly different lifetimes, stability in air, and temperature dependence. Such multifaceted photoluminescent behavior is intriguing not only for its uniqueness but also for the practical implications which can be envisaged in a variety of emerging technologies[17] such as bio-imaging, magnetic-field light manipulation, organic electro-phosphorescence, anti-forgery, O_2-sensing, thermo- and mechano-luminescence.

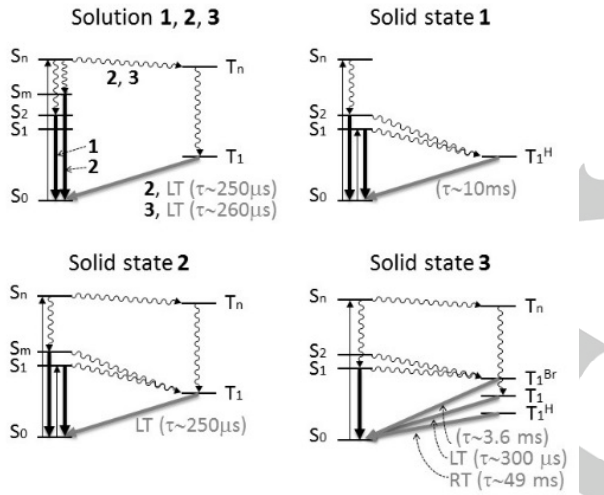

Figure 4. Diagrams displaying the suggested mechanism for fluorescence (black arrows) and phosphorescence (grey arrows) and Table summarizing the emission features of **1**, **2** and **3**.

Acknowledgements

The use of instrumentation purchased through the Regione Lombardia−Fondazione Cariplo joint SmartMatLab Project is gratefully acknowledged. We thank Prof. P. Mussini, Dr. M. Magni and Dr. S. Arnaboldi for CV analysis.

Keywords: H aggregates• halogen bonding • photophysics • room temperature phosphorescence • time resolved spectroscopy

[1] a) S. R. Forrest, M. A. Baldo, D. F. O'Brien, Y. You, A. Shoustikov, S. Sibley, M. E. Thompson, *Nature* **1998**, *395*, 151-154; b) A. Kishimura, T. Yamashita, K. Yamaguchi, T. Aida, *Nat. Mater.* **2005**, *4*, 546-549; c) G. Marriott, R. M. Clegg, D. J. Arndt-Jovin, T. M. Jovin, *Biophys. J.* **1991**, *60*, 1374-1387; d) P. Y. Gu, G. Liu, J. Zhao, N. Aratani, X. Ye, Y. Liu, H. Yamada, L. Nie, H. Zhang, J. Zhu, D. S. Li, Q. Zhang, *J. Mater. Chem. C* **2017**, *5*, 8869-8874; e) P. Y. Gu, Y. Zhao, J. H. He, J. Zhang, C. Wang, Q. F. Xu, J. M. Lu, X. W. Sun, Q. Zhang, *J. Org. Chem.* **2015**, *80*, 3030-3035.

[2] a) E. Cariati, V. Lanzeni, E. Tordin, R. Ugo, C. Botta, A. Giacometti Schieroni, A. Sironi, D. Pasini, *Phys. Chem. Chem. Phys.* **2011**, *13*, 18005–18014; b) T. Virgili, A. Forni, E. Cariati, D. Pasini, C. Botta, *J. Phys. Chem. C* **2013**, *117*, 27161−27166; c) Y. N. Hong, J. W. Y. Lam and B. Z. Tang, *Chem. Soc. Rev*. **2011**, *40*, 5361-5388; d) Z. Y. Zhang, B. Xu, J. H. Su, L. P. Shen, Y. S. Xie, H. Tian, *Angew. Chem., Int. Ed.* **2011**, *50*, 11654-11657; e) B. Wang, Y. C. Wang, J. L. Hua, Y. H. Jiang, J. H. Huang, S. X. Qian, H. Tian, *Chem. Eur. J.* **2011**, *17*, 2647-2655; f) J. Mei, Y. Hong, J. W. Y. Lam, A. Qin, Y. Tang, B.Z. Tang, *Adv. Mate*r. **2014**, *26*, 5429-5479.

[3] a) S. Hirata, *Adv. Optical Mater.* **2017**, *5*, 1700116; b) M. Baroncini, G. Bergamini, P. Ceroni, *Chem. Commun*., **2017**, *53*, 2081-2093; c) W. Zhao, Z. He, J. W. Y. Lam, Q. Peng, H. Ma, Z. Shuai, G. Bai, J. Hao, B. Z. Tang, *Chem.* **2016**, *1*, 592–602; d) S. Xu, R. Chen, C. Zheng, W. Huang, *Adv. Mater.* **2016**, *28*, 9920-9940.

[4] S. Kuno, H. Akeno, H. Ohtani, H. Yuasa, *Phys. Chem. Chem. Phys.* **2015**, *17*, 15989-15995.

[5] P. Xue, J. Sun, P. Chen, P. Wang, B. Yao, P. Gong, Z. Zhang, R. Lu, *Chem. Commun.* **2015**, *51*, 10381-10384.

[6] Y. Gong, G. Chen, Q. Peng, W. Z. Yuan, Y. Xie, S. Li, Y. Zhang, B. Z. Tang, *Adv. Mater.* **2015**, *27*, 6195-6201.

[7] C. Li, X. Tang, L. Zhang, C. Li, Z. Liu, Z. Bo, Y. Q. Dong, Y.-H. Tian, Y. Dong, B. Z. Tang, *Adv. Opt. Mater.* **2015**, *3*, 1184-1190.

[8] Z. Yang, Z. Mao, X. Zhang, D. Ou, Y. Mu, Y. Zhang, C. Zhao, S. Liu, Z. Chi, J. Xu, Y. C. Wu, P. Y. Lu, A. Lien, M. R. Bryce, *Angew. Chem. Int. Ed.* **2016**, *55*, 2181-2185; *Angew. Chem.* **2016**, *128*, 2221.

[9] S. M. Ali Fateminia, Z. Mao, S. Xu, Z. Yang, Z. Chi, B. Liu, *Angew. Chem. Int. Ed.* **2017**, *56*, 12160–12164.

[10] E. Lucenti, A. Forni, C. Botta, L. Carlucci, C. Giannini, D. Marinotto, A. Previtali, S. Righetto, E. Cariati, *J. Phys. Chem. Lett.* **2017**, *8*, 1894−1898.

[11] Z. An, C. Zheng, Y. Tao, R. Chen, H. Shi, T. Chen, Z. Wang, H. Li, R. Deng, X. Liu, W. Huang, *Nat. Mater.* **2015**, *14*, 685–690.

[12] R. Bhattacharya, S. Ray, J. Ray, A. Ghosh, *Cent. Eur. J. Chem.* **2003**, *4*, 427-440.

[13] T. Itoh, *Chem. Rev.* **2012**, *112*, 4541−4568.

[14] A. Mukherjee, S. Tothadi, G. R. Desiraju, *Acc. Chem. Res.* **2014**, *47*, 2514−2524.

[15] T. Clark, M. Hennemann, J. S. Murray, P. Politzer, *J. Mol. Model.* **2007**, *13*, 291−296.

[16] H. Shi, Z. An, P. Z. Li, J. Yin, G. Xing, T. He, H. Chen, J. Wang, H. Sun, W. Huang, Y. Zhao, *Cryst. Growth Des.* **2016**, *16*, 808−813.

[17] a) D. Chaudhuri, E. Sigmund, A. Meyer, L. Rçck, P. Klemm, S. Lautenschlager, A. Schmid, S. R. Yost, T. Van Voorhis, S. Bange, S. Höger, and J. M. Lupton, *Angew. Chem. Int. Ed.* **2013**, *52*, 13449- 13452; b) P. Xue, P. Wang, P. Chen, B. Yao, P. Gong, J. Sun, Z. Zhang, R. Lu, *Chem. Sci.* **2017**, *8*, 6060–6065; c) Z. He, W. Zhao, J.W.Y. Lam, Q. Peng, H. Ma, G. Liang, Z. Shuai, B. Z. Tang, *Nat. Commun.* **2017**, *8*, 416 doi:10.1038/s41467-017-00362-5.

Table 1. UV-vis Absorption and Photoluminescence data at 298 and 77K.

Sample	298 K					77 K		
	λ_{abs} (nm)	Φ (%)	λ_{em} (nm)	τ	Emission assignment	λ_{em} (nm)	τ	Emission assignment
1 (DCM)	230, 261, 282, 298, 301	17	327, 341, 359 (sh)	3.24 ns[a]	S_2-S_0	338, 352, 373 (sh)	0.047 ns (15.5) 2.03 ns (31.4) 5.71 ns (53.1)[b]	S_2-S_0
1 (pwd)		18	335, 350, 366 (sh)[c]	2.61 ns[e]	S_2-S_0	339, 352, 370 (sh)[c]	1.93 ns[e]	S_2-S_0
			387, 407 429 (sh)[d]		S_1-S_0	394, 413, 437 (sh)[d]		S_1-S_0
			497, 536, 623[d]	5 ms (9.0) 35 ms (21.6) 120.8 ms (51.7) 515 ms (17.7)[f]	T_1^H-S_0	504, 537, 621[d]	11.7 ms (75.2) 42.5 ms (17.5) 227 ms (4.6) 1028 ms (2.7)[f]	T_1^H-S_0
2 (DCM)	230, 237, 262 (vw)	3	328, 342, 358	0.12 ns (62.6) 0.82 ns (37.4)[g]	S_m-S_0	580	78.11 μs (14.0) 284.7 μs (86.0)[h]	T_1-S_0
2 (pwd)		<0.1	326, 345, 365, 382[i]	0.05 ns (67.8) 0.98 ns (32.2)[k]	S_m-S_0	344, 365, 378 (sh)[m]	0.28 ns (28.8) 0.93 ns (71.2)[o]	S_m-S_0
			426, 530[j]	1.42 ns (47.1) 6.34 ns (52.9)[l]	S_1-S_0	457, 492, 530[m]	2.54 ns[p]	S_1-S_0
						573[n]	274.15 μs[h]	T_1-S_0
3 (DCM)	235, 241, 268 (vw), 278 (vw)	<0.1	380	0.87 ns (47.2) 5.80 ns (52.8)[q]	S_1-S_0	575	110.34 μs (20.2) 304.22 μs (79.8)[h]	T_1-S_0
3 (pwd)		14	395, 419, 443	0.30 ns (45.8) 1.06 ns (54.2)[r]	S_1-S_0	409, 434, 462[u]	0.194 ns (12.1) 1.25 ns (62.6) 2.81 ns (25.3)[w]	S_1-S_0
			470	125 μs (66) 1.25 ms (34)[s]	T_1^{Br}-S_0	433 (sh), 461, 484[v]	1.64 ms (30) 4.43 ms (70)[z]	T_1^{Br}-S_0
			553, 600, 646	3.09 ms (13.0) 13.09 ms (71.3) 49.22 ms (15.7)[t]	T_1^H-S_0			
						558[n]	302.38 μs[h]	T_1-S_0

[a] λ_{exc} = 300 nm λ_{em} = 342 nm; [b] λ_{exc} = 300 nm λ_{em} = 339 nm; [c] λ_{exc} = 260 nm; [d] λ_{exc} = 360 nm; [e] λ_{exc} = 300 nm λ_{em} = 348 nm; [f] λ_{exc} = 315 nm λ_{em} = 550 nm; [g] λ_{exc} = 300 nm λ_{em} = 325 nm; [h] λ_{exc} = 280 nm λ_{em} = 580 nm; [i] λ_{exc} = 300 nm; [j] λ_{exc} = 350 nm; [k] λ_{exc} = 300 nm λ_{em} = 365 nm; [l] λ_{exc} = 300 nm λ_{em} = 544 nm; [m] λ_{exc} = 310 nm; [n] λ_{exc} = 280 nm; [o] λ_{exc} = 300 nm λ_{em} = 342 nm; [p] λ_{exc} = 300 nm λ_{em} = 492 nm; [q] λ_{exc} = 300 nm λ_{em} = 380 nm; [r] λ_{exc} = 300 nm λ_{em} = 433 nm; [s] λ_{exc} = 370 nm; λ_{em} = 475 nm; [t] λ_{exc} = 360 nm λ_{em} = 550 nm; [u] λ_{exc} = 375 nm; [v] λ_{exc} = 350 nm; [w] λ_{exc} = 375 nm λ_{em} = 405 nm; [z] λ_{exc} = 300 nm λ_{em} = 500 nm.

Entry for the Table of Contents

COMMUNICATION

Three triimidazole derivatives display multiple emissions covering dual fluorescence, impressively Stokes shifted molecular yellow, supra-molecular blue-green and crystalline ultralong red phosphorescences. The yellow component is associated with the presence of a proper T_n close to a high energy S_n level. The blue-green emission derives from a Br_4-synthon T_1^{Br} level. The red one is attributed to a T_1^{H} level stabilized through H-aggregation.

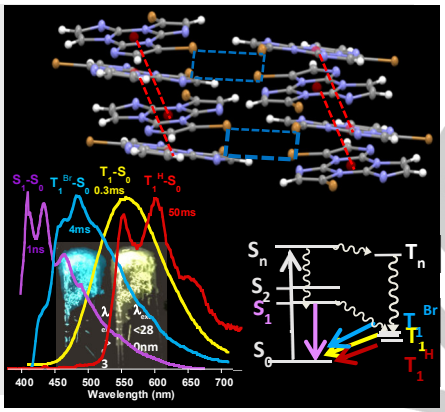

Elena Lucenti, Alessandra Forni, Chiara Botta,* Lucia Carlucci, Clelia Giannini, Daniele Marinotto, Alessandro Pavanello, Andrea Previtali, Stefania Righetto and Elena Cariati**

Page No. – Page No.

Cyclic Triimidazole Derivatives: Intriguing Cases of Multiple Emissions and RT Ultralong Phosphorescence